Heliyon 6 (2020) e03798

Contents lists available at ScienceDirect

Heliyon

journal homepage: www.cell.com/heliyon

Research article

Copper-enriched diamond-like carbon coatings promote regeneration at the bone–implant interface

Peiman Brouki Milan [a,b,c], Sara Khamseh [d], Payam Zarrintaj [e], Bahram Ramezanzadeh [f], Michael Badawi [g], Sophie Morisset [h], Henri Vahabi [i], Mohammad Reza Saeb [j], Masoud Mozafari [a,c,*]

[a] Cellular and Molecular Research Center, Iran University of Medical Sciences, Tehran, Iran
[b] Institutes of Regenerative Medicine, Faculty of Advanced Technologies in Medicine, Iran University of Medical Sciences, Tehran, Iran
[c] Department of Tissue Engineering and Regenerative Medicine, Faculty of Advanced Technologies in Medicine, Iran University of Medical Sciences, Tehran, Iran
[d] Department of Nanomaterials and Nanocoatings, Institute for Color Science and Technology, P.O. Box 16765-654, Tehran, Iran
[e] School of Chemical Engineering, Oklahoma State University, 420 Engineering North, Stillwater, OK 74078, United States
[f] Department of Surface Coatings and Corrosion, Institute for Color Science and Technology, Tehran, Iran
[g] Université de Lorraine and CNRS, LPCT, UMR 7019, 54506, Vandoeuvre-lès-Nancy, France
[h] IC2MP, UMR CNRS 7285, Université de Poitiers, 4 Rue Michel Brunet, Poitiers 86022, France
[i] Université de Lorraine, CentraleSupélec, LMOPS, F-57000 Metz, France
[j] Department of Resins and Additives, Institute for Color Science and Technology, P.O. Box 16765-654, Tehran, Iran

ARTICLE INFO

Keywords:
Biomedical engineering
Materials science
Biomimetics
Tissue engineering
Coatings
Angiogenesis
Osteogenesis corrosion resistance
Copper
Hydrogenated amorphous carbon

ABSTRACT

There have been several attempts to design innovative biomaterials as surface coatings to enhance the biological performance of biomedical implants. The objective of this study was to design multifunctional Cu/a-C:H thin coating depositing on the Ti-6Al-4V alloy (TC4) *via* magnetron sputtering in the presence of Ar and CH_4 for applications in bone implants. Moreover, the impact of Cu amount and sp^2/sp^3 ratio on the interior stress, corrosion behavior, mechanical properties, and tribological performance and biocompatibility of the resulting biomaterial was discussed. X-ray photoelectron spectroscopy (XPS) revealed that the sp^2/sp^3 portion of the coating was enhanced for samples having higher Cu contents. The intensity of the interior stress of the Cu/a-C:H thin bio-films decreased by increase of Cu content as well as the sp^2/sp^3 ratio. By contrast, the values of Young's modulus, the H^3/E^2 ratio, and hardness exhibited no significant difference with enhancing Cu content and sp^2/sp^3 ratio. However, there was an optimum Cu content (36.8 wt.%) and sp^2/sp^3 ratio (4.7) that it is feasible to get Cu/a-C:H coating with higher hardness and tribological properties. Electrochemical impedance spectroscopy test results depicted significant improvement of Ti-6Al-4V alloy corrosion resistance by deposition of Cu/a-C:H thin coating at an optimum Ar/CH_4 ratio. Furthermore, Cu/a-C:H thin coating with higher Cu contents showed better antibacterial properties and higher angiogenesis and osteogenesis activities. The coated samples inhibited the growth of bacteria as compared to the uncoated sample ($p < 0.05$). In addition, such coating composition can stimulate angiogenesis, osteogenesis and control host response, thereby increasing the success rate of implants. Moreover, Cu/a-C:H thin films encouraged development of blood vessels on the surface of titanium alloy when the density of grown blood vessels was increased with enhancing the Cu amount of the films. It is speculated that such coating can be a promising candidate for enhancing the osseointegration features.

1. Introduction

The people all around the world suffer from traumatic injuries causing by accidents, infection and disease-what underlines the demand for orthopedic implants [1, 2, 3]. In this regard, various types of biomaterials have been developed to repair the bone defects [4, 5, 6, 7]. There has been continued attempts to integrate abilities of different biomaterials into the bone tissue engineering realm, mainly based on osseointegrated implants known for the biocompatibility, mechanically durability, and ability to resist against corrosion in biological milieu [8,

* Corresponding author. M. Mozafari, Currently at: Lunenfeld-Tanenbaum Research Institute, Mount Sinai Hospital, University of Toronto, Toronto, ON, Canada.
E-mail address: mozafari.masoud@gmail.com (M. Mozafari).

https://doi.org/10.1016/j.heliyon.2020.e03798
Received 8 May 2019; Received in revised form 17 November 2019; Accepted 14 April 2020

9, 10]. Bone implants featuring appropriate osseointegration should exhibit proper anti-bactericidal features to prevent infection that causes severe consequences, e.g. ca. 37% of infection patients undergo delayed unions and ca.14% need amputation [11, 12, 13].

Titanium (Ti) and derivatives have been utilized so far as the most favorite implants in bone tissue engineering because of proper biocompatibility, low specific weight and moderate corrosion resistance. Nevertheless, suboptimal surface feature of such implants regarding bioactivity acts as Achilles' heel. Hence, architecting materials surface can boost the implants and scaffolds performance in the body [14, 15, 16]. Various types of materials from polymers [17, 18] to metal [19] can be developed and modified to achieve miscellaneous properties like antibacterial feature [20, 21], controlled drug release [22, 23], electroactivity [24, 25], physical properties [26, 27] and biocompatibility [28, 29, 30].

Carbon based films especially amorphous carbon attracted some attentions as multifunctional films in mechanical and biological applications because of their proper chemical feature, corrosion resistance, biocompatibility, hemocompatiblity and physical and biological properties [31, 32]. In spite of their numerous valuable properties, hydrogenated amorphous carbon films (a-C:H) suffer from inadequate adhesion to the metals. The main reason for the low a-C:H adhesion to metal substrates is the high amount of internal stress forms in the film during its deposition. Moreover, lacks of bioactivity of DLC limit its usage in implants usage. Elements doping is one of the main methods which can solve this problem. Dopant elements in the a-C:H coating assist in the graphitization enhancement of carbon layer, which decreases the internal stress [33, 34].

It has been recognized that the lifetime and performance of a-C:H -based coatings in a biological agent, can be predicted based on its mechanical and electrochemical properties. For instance, in some biological applications the wear resistance of the coated part plays a major role in its performance and life time [35]. Stachowiak et al. declared that hardness is the key factor governing the wear rate of a-C:H films [36]. Corrosion resistance is the other important feature of a-C:H based deposited films determines their performance, stability and life cycle. Bio-engineering films are regularly in interaction with harsh chemical or biological milieu [37]. The protection properties of a-C:H films against corrosive media is related to the quality of the substrate adhesion [38]. Bayón et al. observed appropriate adhesiveness and corrosion protection of Ti doped a-C:H films [39]. Elsewhere, presence of SiN_x interlayer was the reason for improved corrosion inhibition in a-C:H layer [40].

Cu and Ag are known to be antibacterial agents for decades. Cu as a metabolizable agent stays in the body after ingestion compared to Ag and Ag-serum levels increases [41, 42]. Cu-ions exhibited enormously bactericidal feature even at low concentrations. Cu-coated implants exhibits higher cytocompatibility for mammalian cells compared to the Ag-coated ones. The bactericide properties of Cu are owing to the Cu-ions release which reduce the use of antibiotics and antiseptics [43, 44]. It is confirmed that Cu-suspension or Cu-coated reduce the bacteria [45]. Moreover, it is noticed that Cu addition affected the mechanical and physical features of a-C:H films [46]. For example, it was reported that Cu increment caused to improving the hardness and adhesiveness of a-C:H film to the metallic surface [47]. Several reports addressed the importance of having an optimum Cu content with particular domain size to meet mechanical properties and hemocompatibility requirements in the magnetron-sputtered Cu/a-C:H coating on magnesium surface [48]. However, no much attention is paid to the corrosion behavior and biocompatibility of Cu/a-C:H coated Ti substrates, in spite of its importance for the use of this film in either chemical or biological environment. On the other hand, it is important for an implant surface to have angiogenic and osteogenic activity to enhance the differentiation of undifferentiated cells especially towards osteoblasts [49].

Based on the aforementioned discussion, there was a need for a-C:H -based coatings to design advanced a-C:H films. Typically, the life time and the performance of a-C:H -based coatings in a biological agent are functions of mechanical, electrical, and chemical characteristics. However, it was revealed that there is a close correlation between microstructure and mechanical/electrochemical feature of the coating. A preferred microstructure is the outcome of a precise design of deposited films. For instance, it has been proved that metal presence in a-C:H matrix help the creation of sp^2 bonded carbon positions; moreover, the dominance of sp^2 makes adhesion improved [50]. This research study tried to address the impact of Cu addition and sp^2/sp^3 fraction on mechanical properties and biological response of a-C:H coatings. The morphology, electrochemical, mechanical and biological features of Cu/a-C:H thin coating were also examined. The optimized morphology could ensure high mechanical properties, high electrochemical stability in biological agents (SBF) and acceptable biocompatibility. Therefore, both bulk and surface properties were imaged on microscope to find a correlation between elemental composition on the surface of coatings with the mechanical, electrochemical and biocompatibility characteristics.

2. Experimental procedure

2.1. Deposition of multifunctional Cu/a-C:H thin coating on Ti discs

A planar style magnetron sputtering equipment, (Yarenikane salehDRS320) was used to prepare Cu/a-C:H thin films. Prior to deposition, a vacuum with pressure of 3×10^{-5} Torr was applied in the apparatus. A mixture of argon and methane, respectively identified as working and reactive gases was charged into the system to sputter copper target varying the CH_4/Ar ratio in 0.2–1.0 A interval. A mirror-polished Ti-6Al-4V alloy coupons equipped with micro-scale glass slides of 20 × 20mm^2 was the substrate on the grounded platform as holder. Prior to sputtering deposition, the platform were rinsed with acetone and alcohol applying ultrasonication. By fixing the distance between the target and the substrate (110 mm), the temperature of substrate raised to 150 °C to bombard the substrate by the particles of target for the duration of deposition without the need for bias application and heating the substrate. By adjusting the sputtering time, films 850–900 nm in thickness of were formed on the substrate (parameters of the test are given in Table 1).

2.2. Characterization of Cu/a-C:H- coated Ti disc surfaces

Electron probe microanalysis (EPMA) (JEOL, JXA-8530F) was used to measure the elemental composition of the sputtered thin coating. The chemical composition of the Cu/a-C:H composite thin coating was examined by an Axis Ultra photoelectron spectrometer with a monochromatic Al Ka (h m 5 1486.6 eV) X-ray source. All peaks were calibrated regard to the C 1s reference peak (283.99 eV). The deconvolution of the high-resolution spectra done by the aid of a computer procedure (Kratos Analytical, Manchester, U.K.).

The interior stress of the thin coating was measured employing a surface profilometer working on the basis of Stoney's equation. Ultra Nanoindentation Tester (UNHT) commercialized by Anton-Paar was used to study the mechanical properties of thin films.

To qualitative and quantitative evaluation of surface morphology and roughness of the prepared films, atomic force microscopy (AFM) was

Table 1. Deposition parameters including sputtering pressure, the thickness and the surface roughness of the coating as a function of Ar/CH_4 ratio.

Sample No.	Sputtering Pressure (Toor)	Ar/CH_4 Ratio	Film's thickness (nm)	Surface Roughness (nm)
T-1	1.5×10^{-2}	1	850 ± 2	0.52
T-2	1.5×10^{-2}	1.5	850 ± 5	1.2
T-3	1.5×10^{-2}	2.3	850 ± 3	1.7
T-4	1.5×10^{-2}	4	850 ± 2	2.1
T-5	1.5×10^{-2}	9	850 ± 3	4

Table 2. Chemical composition of SBF solution used in the EIS measurement as corrosive media.

NaCl	KCl	$CaCl_2$	$NaHCO_3$	$MgCl_2.6H_2O$	KH_2PO_4	$MgSO_4.7H_2O$	$Na_2HPO_4.2H_2O$	Glucose
8 g/L	0.4 g/L	0.18 g/L	0.35 g/L	0.48 g/L	0.1 g/L	0.06 g/L	0.1 g/L	1 g/L

performed on an AFM, Park Scientific Instrument (PC). The bulk morphology of Cu/a-C:H thin coating was imaged on a Mira (field emission-scanning electron microscope (FE-SEM-modelTescan)) microscope via scanning electron microscopy (SEM).

Ti-6Al-4V alloys coated with Cu-enriched DLC coatings were subjected to corrosive media to assess their corrosion resistance on an electrochemical impedance spectroscopy (EIS) model Ivium Compactstat. The test was conducted in a three electrode cell including Ag/AgCl (3 M KCl) as control, graphite rode as counter and the Ti-6Al-4V alloy samples, with and without coating, as working electrode. The coated and uncoated samples (1 cm^2) were dipped in a simulated body fluid (SBF) solution (with the chemical composition given in Table 2) for various times. An open circuit potential (OCP) with 10 mV perturbation was used to perform measurements in the frequency range of 10 kHz-10 mHz.

2.3. Cell culture and quantitative real-time PCR assay

The human bone marrow derived stem cells (hBMSCs) were prepared from the IUMS research center and cultured in a 10 mL dish of a-MEM (Gibco) supplemented with 10% Fetal bovine serum (FBS) and 1% Penicillin/Streptomycin (Sigma Aldrich), and cultured at 37 °C in a humidified incubator with 95/5 v/v air/CO_2 circulation. All experiments were done within passage 3. The cell suspension of 500 μl containing 2×10^4 cells was seeded on the implants.

After incubation of cells with osteogenic media after 21 days, the total RNA has been extracted from hBMSCs utilizing the RNAeasy Mini Kit (Qiagen, USA)., and then the purified RNA was placed in 6-well plates and reversed transcribed into cDNA using a RevertAid First Strand cDNA Synthesis Kit (Lithuania). Then, samples have been cleaned with DNAse I amplification grade (Invitrogen) to remove the contaminatedgenomic DNA from the RNA. Glyceraldehyde-3-phosphate dehydrogenase (GAPDH) was selected as a housekeeping endogenous control gene. The mRNA levels of the osteogenic marker genes included alkaline phosphatase (ALP) and the osteocalcin (OCN)) profiling (SYBRPremix ExTaqII (Qiagen) as well as VEGF as an angiogenic marker were quantified by a quantitative real-time polymerase chain reaction (RT-PCR) with specific primers.

The test was conducted on a Rotor-GeneTMSYBER Green PCR Kit (Qiagen, USA) in accordance with the protocol proposed by the manufacturer. The heating cycle was stratted by an primary denaturation step at 95 °C for 10 min, and overall 40 cycles were run at 95 °C for 30 s; 60 °C for 30 s; and 72 °C for 30 s. The 2-delta-delta- Ct (2-DDCt) methodology [45] was applied to calculate the quantification in gene expression. The primers used for the target genes are presented in Table 3.

2.4. Antibacterial test

Bacteria culture; Porphyromonas gingivalis (ATCC 33277, provided by the laboratory center, Institue pasture, Tehran, Iran), which is most frequently associated with subgingival and peri-implant infections [51] was cultured on blood agar plates augmented with 5% defibrinated sheep blood (Thermo Scientific™, R54020) under standard anaerobic conditions.

The sterile implants were rinsed with distill water three times and sterilized with gamma irradiation, then placed in 6-well culture plate with the coated surface facing upward, and separately incubated with 5ml of P. gingivalis (1×10^7 CFU/mL) for 48h, in Fastidious anaerobe broth (Thermo Scientific™, CM0957). The plates were later wrapped with a parafilm to avoid any contamination. The negative and positive controls were respectively the blank and cultured Cu/a-C:H coated and uncoated Ti implants. The antibacterial properties of the prepared implants were studied using laser scanning confocal microscopy (ZEISS LSM 980). Biofilm bacteria were measured using a red nucleic acid probe (the SYTO 60, Eugene). The Biotinylated Aleuria Aurantia Lectin (Vector B-1395) was also used to label Glycoconjugates of biofilms and then stained using the Alexa-488 staining kit in line with manufacture data sheet. Next, a biofilm area of about 2–3 cm2 was isolated from the disc and then placed in a sterile plate. The specimen was then incubated at 37 °C for 30 min with 300 ml of the Alexa-488 labeled lectin (1:10 diluted stock solution). The surface of the specimens washed three times with the PBS. Finally, the samples were treated with red probe and evaluated by laser scanning confocal microscopy (ZEISS LSM 980, Germany). Laser excitation and Emission signals were 488nm, 550 nm (lectin) and 633nm and 650nm (SYTO 60), respectively. Each group was analyzed at three locations. The ImageJ software was used to quantify 3-dimensional data.

2.5. In vivo biocompatibility evaluation

Animal studies were conducted at the Center for Experimental and Comparative Studies at Iran University of Medical Sciences (The approval issued by Ethics Committee of Iran University of Medical Sciences). The host tissue response and angiogenesis activity of uncoated and Cu/a-C:H coated implants was evaluated after subcatanous implantation. Fifteen New Zealand white male rabbits (ca. 2.75 kg) were housed sterilized in individual cages in a standard animal laboratory as per the Iran University of Medical Sciences Council on Animal Care Guidelines. For in vivo study, the rabbits randomly divided into five groups (n = 3 each), designed T1 to T5. All implants were sterilized using gamma irradiation, and subsequently implanted at subcutaneous dorsum following anaesthetization with ketamine (25 mg/kg) and (xylazine 5 mg/kg).

2.6. Histological and immunohistochemistry

Two weeks after the operation, rabbits have been sacrificed during 7% CO_2 inhalation. The surgery sites were dissected, and the implant-containing subcutaneous tissue were harvested and immediately fixed with 4% paraformaldehyde and embedded in paraffin wax. The prepared embedded tissue samples were then sectioned 6 μm. Then, the sections have been marked with Hematoxylin and Eosin (H&E, Sigma-Aldrich, USA). Microscopic images were visualized under a light microscope (OLYMPUS IX81; Olympus, Japan).

Table 3. The feature of primers utilized for real-time PCR evaluation.

Accession No.	Gene	Forward primer sequence	Reverse primer sequence
NM 000487	ALP	5′-CACGTCGATTGCATCTCTGG-3′	5′-GCCAGTACTTGGGGTCTTTC-3′
NM 199173	OCN	5′-ACCATGAGAGCCCTCACACTCCT-3′	5′-GTCTCTTCACTACCTCGCTGCC-3′
NM 001025366.2	VEGF	5′-ACCATGAACTTTCTGCTGTCTTG-3′	5′-ACATCCATGAACTTCACCACTTC-3′
NM 138400	GAPDH	5′-ATCAAGTGGGGTGATGCTGG-3′	5′-TACTTCTCGTGGTTCACGCC-3′

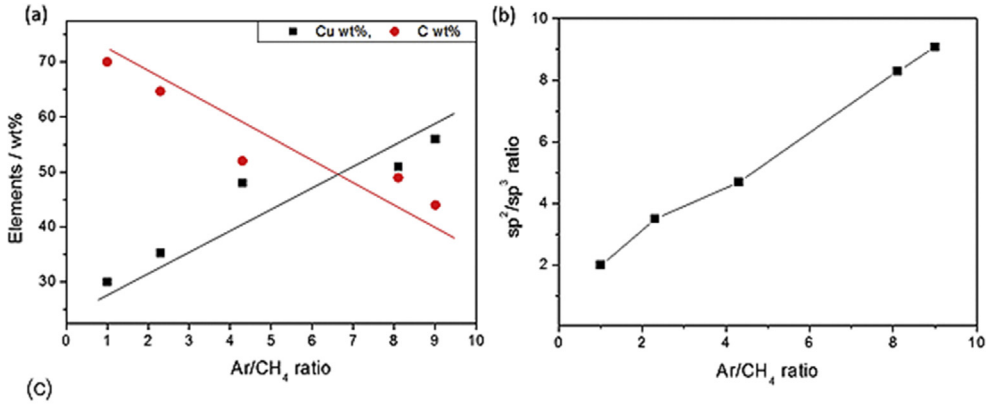

(c)

Ar / CH_4 ratio	O (at%)	C (at%)	Cu (at%)	N (at%)	Si (at%)
1 (sample C1)	11.8	85.5	1	-	1.6
0.8 (C2)	6.2	92.6	-	-	1.2
0.6 (C3)	11.6	87.3	-	-	1.1
0.4 (C4)	11	87.1	-	-	1.9

Figure 1. Influence of Ar/CH_4 ratio on the elemental surface composition (a) and sp^2/sp^3 proportion (b) of the Cu/a-C:H sputtered coatings measured using electron probe microanalysis (EPMA); and the elemental composition acquired by XPS at high resolution (c).

To monitor the angiogenic potential of the samples in vivo, the expression of CD 31 marker was evaluated utilizing immunohistochemistry staining. For this reason, the paraffinized slides were conditioned for 10 min by deparaffinization, rehydration, and incubation in the 3% hydrogen peroxide/methanol solution. To treat the slides for making antigen retrieval, a citrate buffer solution was used and conditioned in an oven for further 10 min. Next, the slides underwent permeabilization in 0.3% Triton X-100 for 0.5 h followed by incubation in 10% normal goat serum to block non-specific binding sites. Incubations with the primary antibodies of anti-Osteocalcin Mouse monoclonal (ab13418, Abcam, UK), anti-Alkaline Phosphatase Mouse monoclonal (ab17973, Abcam, UK), and anti-VEGF Mouse monoclonal (ab1316, Abcam, UK) antibodies were carried out at 4 °C for 24 h. The resulting surfaces were washed three times using PBS solution, the tissues were incubated with Alexa Fluor conjugated goat anti-mouse (ab175660, Abcam, UK) for 60 min at 37 °C, and rinsed with PBS. Then, the slides were stained with propidium

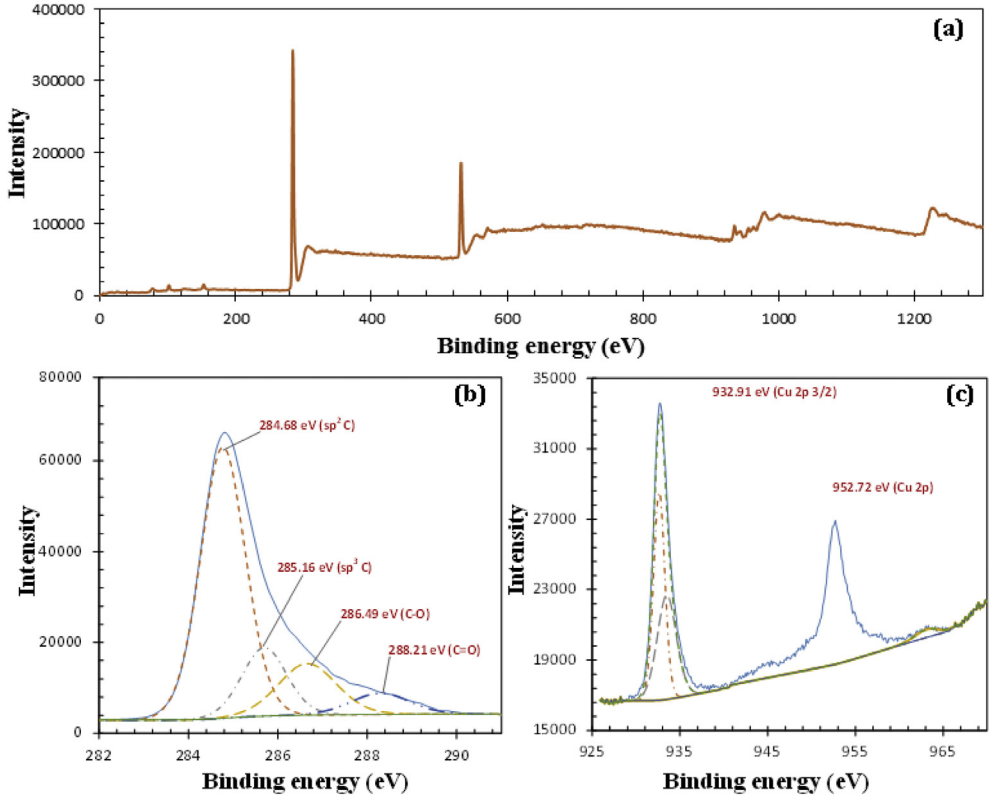

Figure 2. XPS analysis of the elemental composition of the Cu/a-C:H coated Ti-6Al-4V substrates varying the Ar/CH_4 ratios.

iodide (PI), which specifically bonded to nucleus and visualized with fluorescent microscopy (BX53 Upright Microscope, Olympus Life Science Solutions, Japan). Eventually, the IHC-stained samples were quantified on an Image J software (Version 1.4).

3. Results and discussions

3.1. Characterization of Cu/a-C:H –coated implants

Elemental weigh composition of Cu and C in the Cu/a-C:H sputtered layer on the Ti-6Al-4V substrate was detected and plotted in terms of Ar/CH_4 in Figure 1(a). The concentration of Cu in the films rose from 30 to ca. 55 wt.% by 50% as a result of increase of Ar concentration in the gas mixture from 50% to 90%. This is while the weigh composition of C in the coating experienced a decline from 70 to 45 wt.% by ca. 36%, suggesting successful deposition of Cu target on the substrate [52]. The sp^2/sp^3 ratio of the C-C bond in the Cu/a-C:H films followed an ascending trend by increase of Ar/CH_4 ratio in Figure 1(b) demonstrating enhanced graphitization with low amount of diamond-like sp^3 bonding. Incorporation of Cu into the deposited layer is the reason for sp^2 bonded carbon sites [53]. From Figure 1(c), it can be recognized that the sp^2 bonded carbons are abundant, which decreases the internal stress and boosts adhesion of thin film to the substrate Figure 1(c).

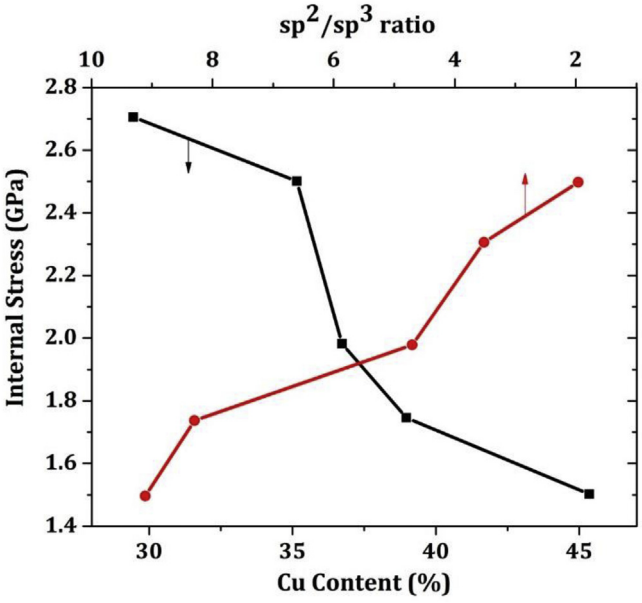

Figure 3. Internal stress of the Cu/a-C:H coatings as a function of Cu content as well as the sp^2/sp^3 ratio in the film.

The surface elemental composition of the Cu/a-C:H coated Ti-6Al-4V substrates with different Ar/CH_4 ratios has been measured using XPS analysis. The typical overall XPS evaluation and high resolution C 1s and Cu 2p peaks for the Ar/CH_4 ratio of 4.3 are presented in Figure 2. According to Figure 2, two peaks are appeared at 932.91 and 952.72 eV, which are characteristics of the Cu, assigned to the broad Cu 2p 3/2 and Cu 2p, respectively. The C 1s signal was deconvoluted into four peaks having binding energies of 284.68, 285.16, 286.49 and 288.21, respectively ascribed to the sp^2 C, the sp^3 C, the C-O and the C=O. The ratio of C (sp^2)/C (sp^3) is 4.76, indicating that the film deposited is mostly composed of graphitic structures. Moreover, the area below the peaks was calculated showing that the film contains 54% C (sp^2), 30% C (sp^3), 7% C-O and 8% C=O, suggesting that graphitic compounds are partially oxidized.

Figure 3 shows the compressive internal stress of coatings in terms of Cu content and the ratio of sp^2/sp^3. The value of the internal stress slightly decreased from 2.7 to 2.5 GPa upon increase of Cu weight prevent from 30 to a bit above 35%, followed by a sudden drop down to 1.5 GPa by further increase of Cu content in the coating, slightly above 45 wt.%. In a similar manner, Cu content decreased by increase in the sp^2/sp^3 ratios. This is mainly because of formation of sp^2 bonded carbon sites upon doping more metal in the coating structure or because of the majority of graphitic domains resisting against internal stress dominance [53, 54].

The texture and the roughness characteristics of the surface of coatings as well as the bulk grained structure of some selected films were imaged on AFM and FE-SEM (Figure 4). Top view of the T-1 sample having the minimum Cu content among the studied thin films was provided by FE-SEM micrograph illustrating the smooth surface being

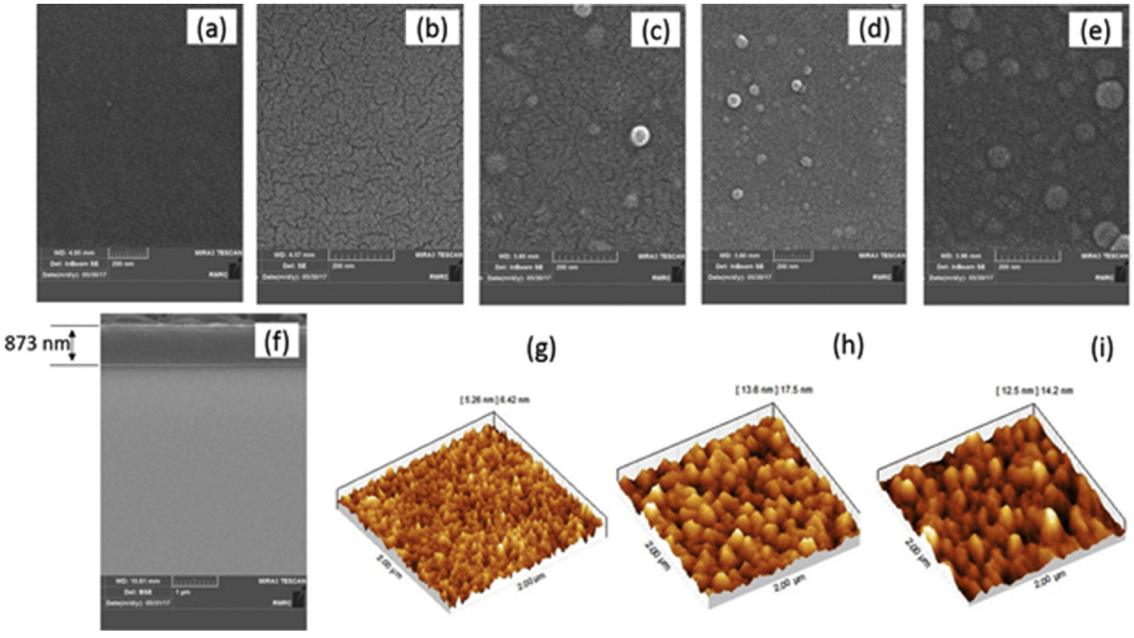

Figure 4. Morphological evaluation of Cu/a-C:H thin coating. SEM of the) a (T-1)b (T-2)c (T-3)d (T-)e (T-5)f (cross section of T-1. AFM image of (g)T-1, (h) T-3 and (i) T-5.

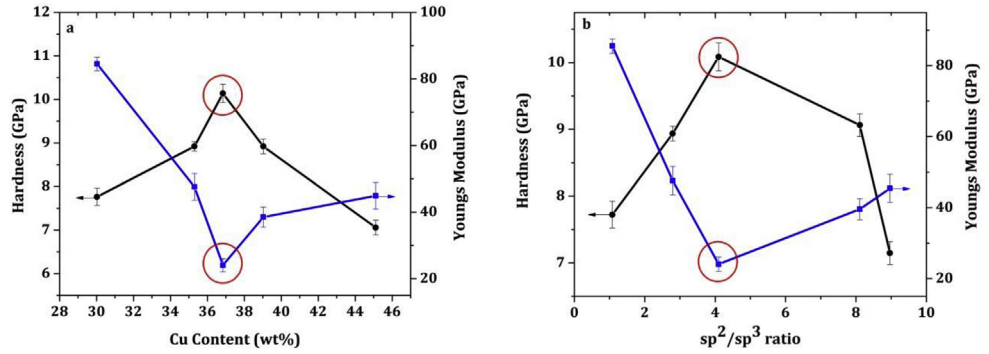

Figure 5. Variation of the hardness and Young's modulus of Cu/a-C:H thin coating in terms of Cu content (a) and sp^2/sp^3 ratio (b).

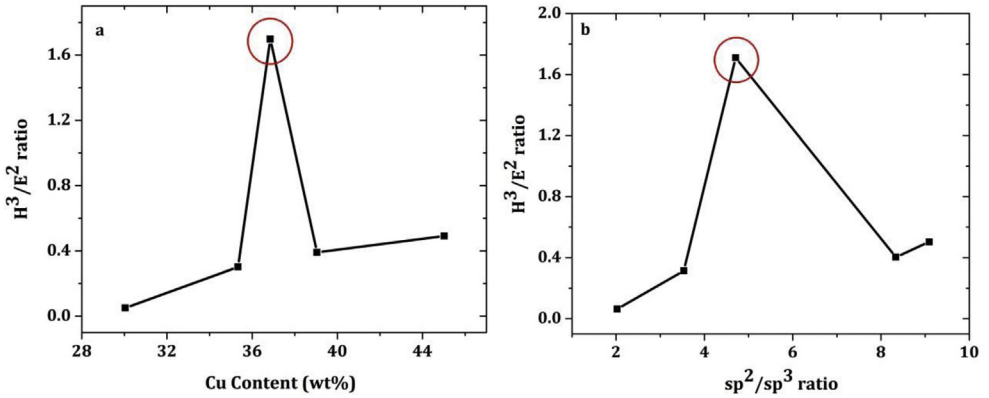

Figure 6. The variation of H^3/E^2 proportion of Cu/a-C:H thin films with Cu content (a) and sp^2/sp^3 ratio (b).

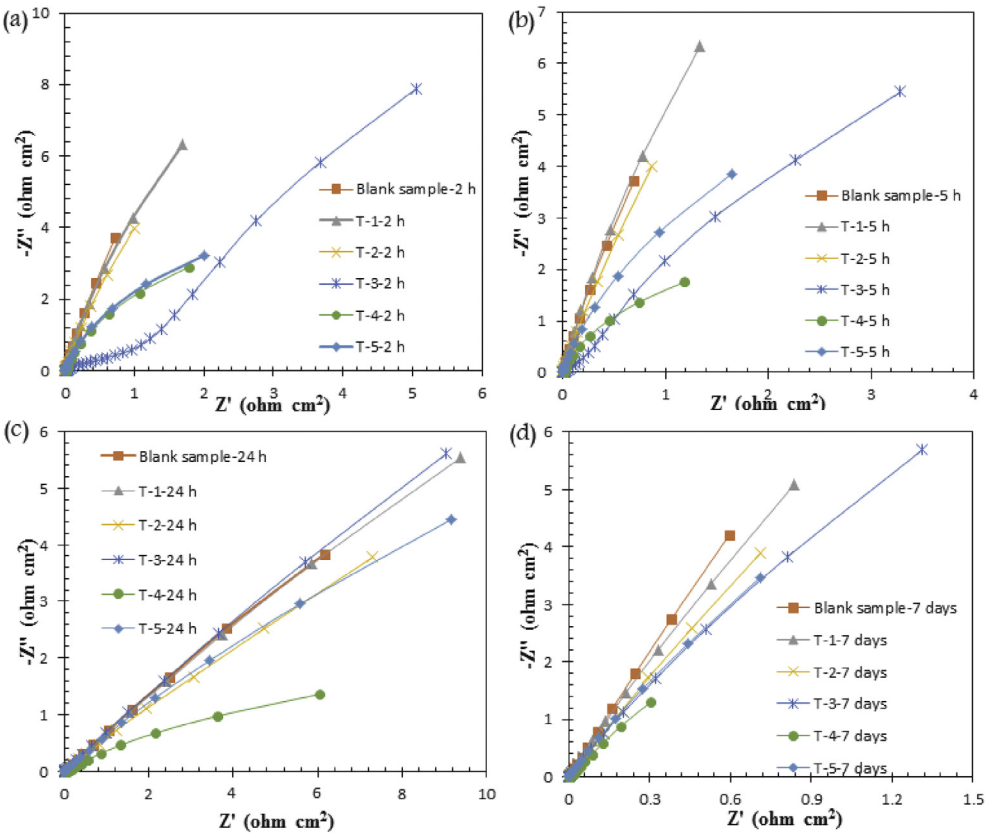

Figure 7. Nyquist diagrams of Ti-6Al-4V samples coated with various Cu/a-C:H coatings. The EIS analysis was performed in SBF solution varying exposing time: (a) 2 h; (b) 5 h; (c) 24 h; (d) 7 days.

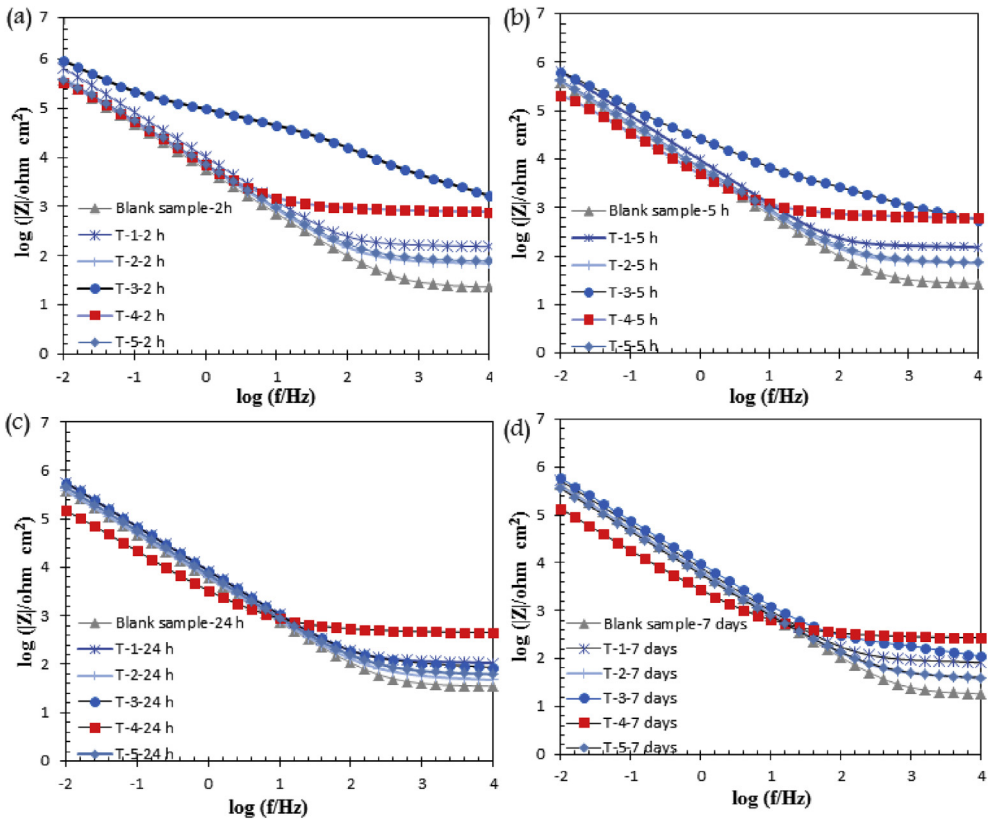

Figure 8. Bode diagrams of of Ti-6Al-4V samples coated with various Cu/a-C:H coatings. The EIS analysis was performed in SBF solution varying exposing time: (a) 2 h; (b) 5 h; (c) 24 h; (d) 7 days.

formed (Figure 4a). A worm-like morphology was observed in T-2 film (Figure 4b), while some round grains were formed on the surface of T-3 film (Figure 4c), typical of thin films of immiscible composites of metal and carbon [55]. It can be seen that the size and the number of round lumpy zones in the surface morphology of samples were increased by increase of Cu content and also with high sp^2 contribution (Figure 4d, e). Moreover, grain size of the samples with lower Cu content and sp^2/sp^3 ratio was smaller and showed higher density (Figure 4a, b). To assess the bulk morphology of samples, cross-sectional microstructure of T-1 specimen was imaged on FE-SEM illustrating a smooth structure with fine grained texture (Figure 4f).

Micrographs provided from the surface of specimens by the AFM approved grain size coarsening of coatings upon increase of Cu concentration and sp^2 contribution (Figure 4g–i). The root mean square (rms) of surface roughness given in Table 1 give a quantitative feeling of roughness alteration.

Figure 5 shows the values of the hardness and Young's modulus of sputtered coatings in terms of Cu wt.% and the ratio of sp^2 to sp^3 ratio. Overall, the behavior of tests over both changing variables are more or less the same, but hardness and Young's modulus are inversely in correlation. There is an optimal trend in both responding variables, so that hardness has peaked at an intermediate concentration of Cu and sp^2/sp^3

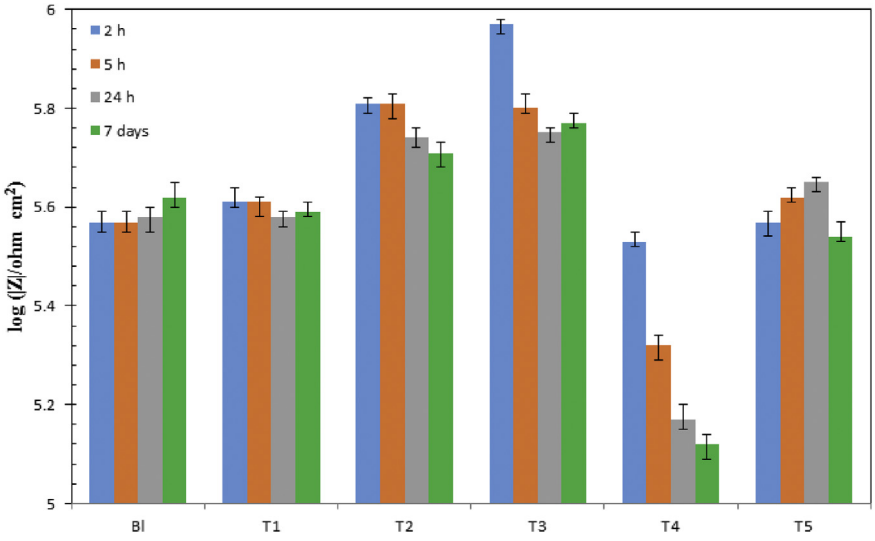

Figure 9. The impedance values, at 10 mHz ($|Z|_{10\ mHz}$), for various samples as a function of immersion time.

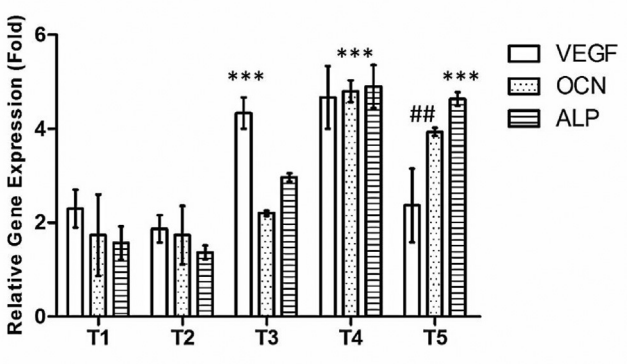

Figure 10. Determination of angiogenesis and osteogenesis. The expression results were normalized to that in normal bone. The microRNA expression of angiogenic marker VEGF and osteogenic markers OCN and ALP assessed in hBMSCs after 21 days of post-treatment. There was a statistically significant discrepancy among groups after 21 days incubating. The VEGF mRNA expression was significantly greater in the T3 and T4 groups in comparison to other groups at days 21. Nevertheless, expression of ALP and OCN were significantly high in the T4 group. A Kruskal-Wallis exam was utilized to verify statistical significances (*$p < 0.05$, **$p < 0.01$, ***$p < 0.001$, and ****$p < 0.0001$). Data are exhibited as mean values ± standard deviation (SD).

ratio, while Young's modulus had minimum value exactly at the same values of changing variables. For hardness, we can see a rise from 7.8 GPa for specimen having 30 wt.% of Cu and at the sp^2/sp^3 ratio of 0.11, to 10 GPa for sample containing 37 wt.% of Cu and sp^2/sp^3 ratio of 0.23. However, hardness was declined at higher Cu and sp^2/sp^3 ratio values. By contrast, the there was a fall in the Young's modulus from 88 GPa for sample having 30 wt.% of Cu and sp^2/sp^3 ratio of 0.11, to 25 GPa for sample with 37 wt.% of Cu and sp^2/sp^3 ratio of 0.23, but increased by further increase of changing variables.

Typically, as the amount of non-carbonic component has a higher contribution to the coating composition, a reduction in the internal stress and consequently in the harness would be expected as a result of enlargement of graphitic domains [56, 57]. Since alteration of the internal stress of Cu/a-C:H coatings was limitedly affected by the Cu content and sp^2/sp^3 ratio, the hardness value of the films revealed a small change. On the bedrock of the minimum Young's modulus and maximum harness featured by T-3 thin film at Cu content of 37 wt.% or the equivalent sp^2/sp^3 ratio of 0.23, formation of nanocomposite structure can be speculated [58, 59]. When there are two immiscible elements in the coatings system (here Cu and a-C:H), a nanocomposite can be formed at an optimum composition due to diffusion rate controlled or spinodal phase segregation [60]. In this case, nanocrystals of one phase are covered with a monolayer of ca. 0.3–0.5 nm in thickness of the second phase (amorphous tissue) [46, 55]. Thermodynamically, Cu and carbon form an immiscible blend at a critical composition through spinodal decomposition mechanism [55, 61]. It is well-documented that the hardness of the coating increases when a nanocomposite structure comes into exist, for no grain boundary is formed; therefore no defect exists in the thin film to deteriorate the hardness [46].

Figure 6 shows alteration of H^3/E^2 ratio of the Cu/a-C:H coatings as a function of the content of Cu and the ratio of sp^2/sp^3. The higher the H^3/E^2 ratio, the more the resistance of coatings against plastic deformation. Similar to the case of hardness and Young's modulus, at the critical Cu content of 37 wt.% (sp^2/sp^3 ratio of 0.23), T-3 sample gives an optimum value of ca. 1.7 for H^3/E^2 ratio. Therefore, controlling the content of Cu and graphitization by altering the Ar/CH_4 ratio applied in sputtering, it is possible to simultaneously control the tribological and mechanical properties of the thin coatings.

The corrosion resistance of Ti-6Al-4V alloy samples, coated by various Cu/a-C:*H thin films, was studied by* EIS analysis in SBF solution for various times. The Nyquist and Bode graphs are provided and shown in Figures 7 and 8.

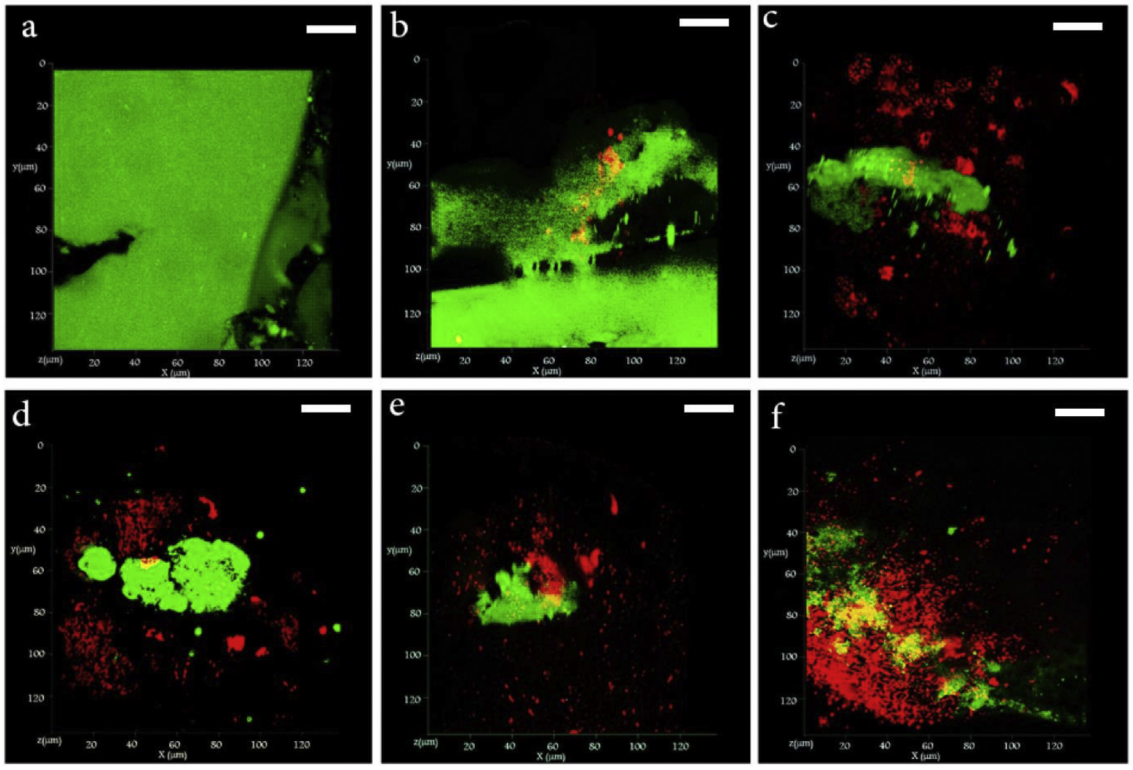

Figure 11. Confocal laser scanning microscopy imaging a) control b)T-1 c) T-2 d) T-3 e) T-4 f) T-5. High number of dead cells (red) was detected in the T 2 and T5 groups. Scale bar = 200μm.

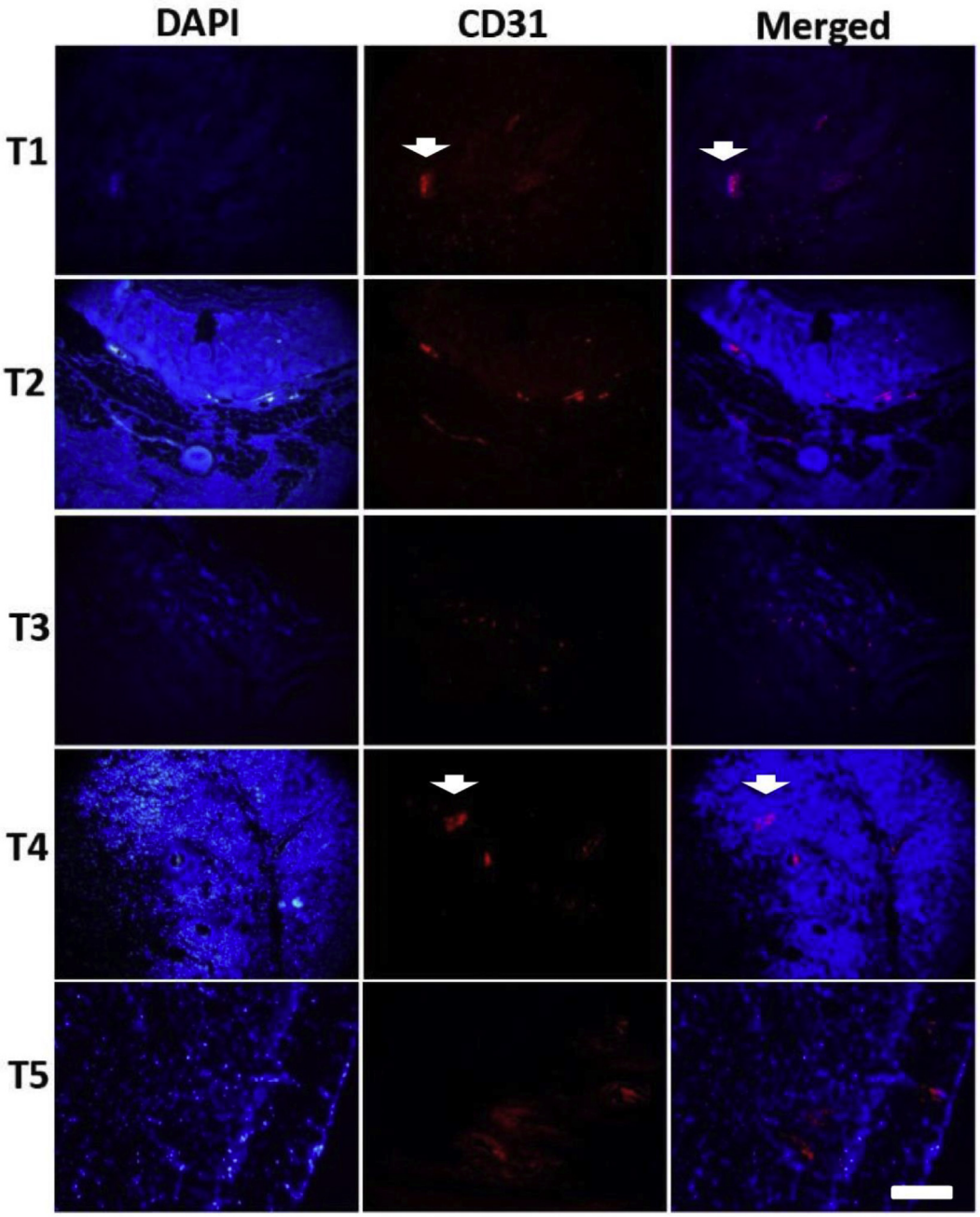

Figure 12. Mmunohistochemical analysis CD31 protein marker (red) as a angiogenesis specific marker at days 21. The analysis exhibited angiogenesis enhancement in t groups due to high amount of copper in this sample. The expression of proteins CD31 was detected through Alexa Fluor conjugated goat anti-mouse (red dots) and Cell nuclei were stained with Dapi (blue dots).

It can be seen from the EIS results that the Nyquist and Bode plots of all samples include one relaxation time except the T-3 sample (at 2 and 5 h immersion) (Ar/CH_4 ratio of 2.3). This indicates that charge transfer determines the corrosion behavior of the reference Ti-6Al-4V alloy and its coated T-1, T-2, T-4 and T-5 samples are under charge transfer control. A distinctive second time constant can be observed at high frequency range in the impedance plots of the Ti-6Al-4V alloy coated with Ar/CH_4 ratio of 2.3. The time constant at high frequency is attributed to the Cu/a-C:H thin coating deposited on the alloy surface. Observation of the time constants of coatings for T-3 sample indicate that the film deposited at this condition (Ar/CH_4 ratio of 2.3) is barrier enough against corrosive agents existed in the SBF solution to the Ti alloy surface. The time constant of the thin coatings sputtered on the T-3 sample can be detected up to 5 h corrosion media exposure but further increment of immersion time caused to the disappearance of this time constant. Decline in the diameter of the first loop in the Nyquist plots of T-3 sample is attributed to the deterioration of coating that detriments barrier properties. Figure 9 compares the impedance values of specimens at 10 mHz ($|Z|_{10\ mHz}$).

Overall, increasing the test time led to increase in the $|Z|_{10\ mHz}$. By increasing the Ar/CH_4 ratio from 1 to 2.3, a significant increase was observed in the $|Z|_{10\ mHz}$ compared to the bare Ti alloy sample. A decreasing trend for $|Z|_{10\ mHz}$ was seen at higher Ar/CH_4 ratios (T-4 and T-5). The best anticorrosion performance was seen for T-3 sample. Not only the morphology of the film deposited but also the chemical composition are important factors affecting the corrosion resistance of deposited film. The graphitic structures are less defected and more impermeable against diffusion of electrolyte. It seems that there is an optimum sp^2 fraction and graphitic domain sizes which results in the

increase of adhesion and corrosion resistance. The decrease in corrosion resistance of T-4 and T-5 samples can be attributed to the creation of the films with lower density, defected structures including large size round grains and weaker barrier properties (Figure 9). This may be also attributed to the high Cu contents in the film deposited on the T-4 and T-5 samples. These samples (T-4 and T-5) include Cu rich regions which more positive potential than others, providing galvanic couples and intensifying the corrosion of Ti-reason why T-4 and T-5 samples have lower corrosion inhibition with respect to the bare Ti sample. At Ar/CH_4 ratio of 2.3, the film thickness, adhesion to the substrate and the impermeability are optimum, resulting in the highest corrosion resistance, which approves the hardness test.

3.2. Angiogenic and osteogenic activity

After culturing cells on the samples for 21 days, the gene expression profile in cultured cells are measured using Quantitative real time PCR. Data showed that the VEGF gene expression in cells on the T3 and T4 were significantly higher than other samples at days 21 showing that the Cu incorporation strangely improves the expression of the angiogenic factor. Numerous studies have showed that copper can remarkably stimulate angiogenesis. A generally known mechanism is that Cu can create the hypoxia condition through HIF-1α to initiate the VEGF expression which is accomplished with new blood vessel formation [62, 63].

Cu ions hamper the ubiquitin-proteasome pathway and prevent the HIF-1α degradation and stabilize it. Moreover, it has been known that creation of and binding of the HIF-1 transcriptional complex to the hypoxia responsive elements (HRE) sequence target genes was enhanced by Cu ions [64]. It has been hypothesis that, hypoxic tension in cellular environment especially in the bone and marrow cause to HIFs expression and response to HIF activation which can results in osteogenesis and enhancing the accumulative VEGF in bone. VEGFR (VEGF receptors) on endothelial cells stimulate angiogenesis and enhance the oxygen and nutrient supplies which can ameliorate osteogenesis indirectly. Moreover, VEGF can interact directly with osteoblasts and enhance the osteogenesis [65].

In addition, expression of the osteogensis related genes including ALP and OCN were measured after culturing cells on implants after 21 days which is depicted in Figure 10. It can be seen that the OCN and ALP were significantly expressed on the cells cultured on the T4 and T5 samples. These results indicate that Cu has osteogenesis activity.

The healing procedure in the presence of the implant resembles the primary bone healing process. Blood clot is formed and transformed by phagocytic cells, such as polymorphonuclear leukocytes, lymphoid cells, and macrophages. After one day to three day after surgical operation, phagocytic activity reaches to the highest point which the bone remodeling happens with prosthesis attachment. Bone is stimulated with stresses. In dental applications, after bone remolding and osseointegration, osseointegrated implant can tolerate the satisfactory and occlusal stresses and distribute the stress appropriately.

3.3. Antibacterial activity

The antibacterial activity of Cu/a-C:H –coated titanium implants is shown in Figure 11 Antibacterial evaluation by imaging analyzing (confocal microscopy) results further demonstrated that Cu/a-C:H –coated titanium implants could inhibit bacterial growth and biofilm formation. Cu/a-C:H-coated titanium implants were most effectively suppressed and killed bacteria in comparison with uncoated implants (as represented by the red stained bacteria amongst the green stained biofilm in Figure 11). The bactericide activity of Cu/a-C:H –coated titanium implants against Porphyromonas gingivalis, increased with increasing Cu content.

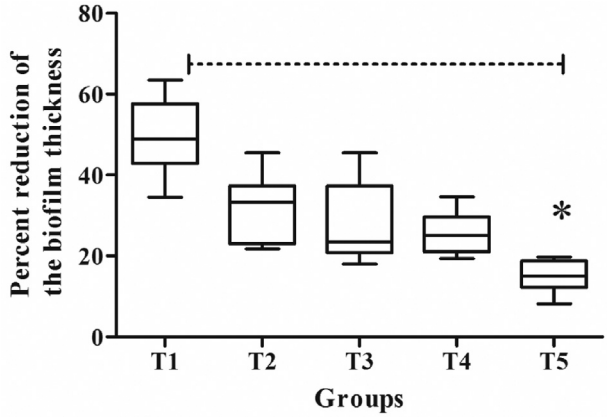

Figure 13. The biofilm percentages have been calculated for each group using image J software. Data are shown as mean values ± standard deviation (SD). (*$p < 0.05$).

In addition, no meaningful variance was detected between the control and treated groups within the expression of the CD31. It can be seen from the Figure 12.

It can be seen, there was a significantly decline in the biofilm thickness of the T5 sample when compared to the uncoated surfaces after 72h incubation. Figure 13 illustrates the percent reduction of the biofilm thickness of all the sample as compared to the uncoated control sample.

In Cu/a-C:H composites, it has been speculated two mechanisms for bactericidal properties. The primary mechanism attributes to the physical interaction of carbonaceous nanoscale substrate with bacteria which bacteria exposed with irrecoverable damage of outer membrane of cell resulting in exuding intracellular content [66]. Structure and chemical bonds of diamond like carbon structure affect the bacterial adhesion to the substrate because of surface free energy decrement [67]. Second mechanism attributes to copper ions release from Cu/a-C:H film which usually involves dissolution and diffusion. While the film was contacted with solution, because of the submicron-sized cracks existing within films electrolyte solution can permeate within the film and copper is ionized to copper ions. Chen et al. prepared copper nanoparticles encapsulated by carbon and evaluated the antibacterial activity. It was revealed that the carbon layer capture the bacteria and the copper obliterate them [68]. Javid et al. prepared the Cu:C nanocomposite using plasma and evaluated the antibacterial property. It was understood that such a composite could act against the gram positive and gram negative bacteria [69]. Chan et al. deposited the carbon like diamond and copper on glass substrate using magnetron sputtering which exhibited the antibacterial activity against E. coli [55].

Physiochemical condition anodic dissolution of the metal and cathodicreduction of water resulted in suppressing electron/hole recombination of titanium alloy and thus inducing oxidation and reduction quantum yields [70]. Ions release can inactivate the respiratory enzymes, interrupt the electron transport and cell membrane depolarization [71].

This finding is in agreement with Burghardtt et al (2015) findings which showed antibacterial effects of copper salt-coated titanium implant against planktonic *S. aureus* within 24h [72]. It is encouraging to compare this figure with that found by Wu et al (2013) who found that thin bioactive glass film containing copper has most effective killing activity against species of bacteria existed in the oral cavity [73]. Although a maximum concentration of copper within materials would provide highly augmented antibacterial activity, a balance between this property and other basic performance is critical for selection of the optimum dosage of copper into the coating materials.

Generally, surface chemical composition and roughness are known as the most important factors in bacteria interaction. Roughness enhances the surface area cause to bacteria contact easily to the surface and more

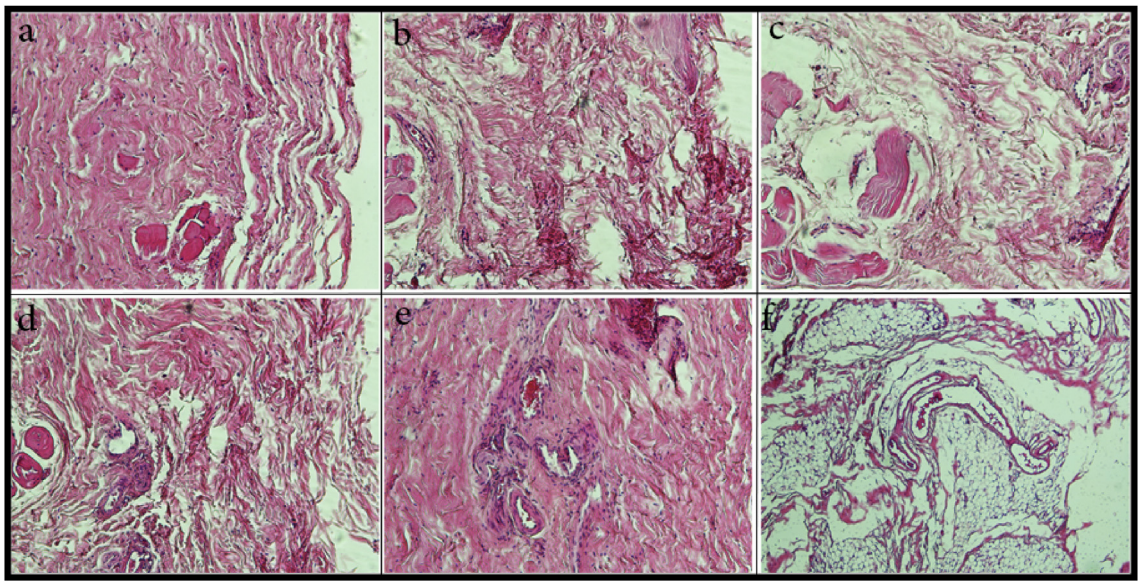

Figure 15. Histological sections obtained from H&E-stained harvested tissue after two weeks post-surgery. a) control, b) T-1, c) T-2, d) T-3, e) T-4, f) T-5.

grooves prepare the appropriate substrate for colonization of bacteria [74, 75]. It should be noticed that, roughness of surface can affect the bacteria colonization in the ranges around 1.0 μm (cell size). In this study, the surface roughness changed from 0.3 to 0.5 nm and the radius of the studied bacteria altered between 0.5 and 2 μm [76, 77]. Hence, it is reasonable that the surface roughness has no significant effect on the antibacterial performance of Cu/a-C:H films.

3.4. Host response evaluations

After two weeks of implantation, we found that both coated and uncoated implants had been surrounded by thin dense connective tissue capsule but the surrounded capsule was only vascularized in Cu/a-C:H implants. Regeneration of blood vessels in the vicinity of coated implants is obvious in macroscopic images.

Figure 15 represents the histological sections obtained from H&E-stained harvested tissue after two weeks post-surgery. Evaluation of the histological data at the fourteen's day after treatment was a signature of intensified regeneration of blood vessels in around each the Cu/a-C:H implants than in the uncoated implants and much denser in the T5 sample. It seems possible that these results are due to existence and increase of copper in the structure of coatings. This finding supports previous research into this area which links copper and angiogenesis. Once the proportion of metal in the alloys has increased, it acted as a pleiotrophic agent assisted in angiogenesis, which eased the release of mediators of angiogenesis [73, 78, 79]. The contribution of Cu to the stimulation of hypoxia-inducible factor-1 (HIF-1) as the transcription factor and its effect on regulating the expression of VEGF was already approved, a platform on which vascular systems in the skeletal muscles can be developed [80].

A recent study by Natalia Mroczek-Sosnowska (2015) reported that copper nanoparticles can stimulate VEGF-A expression and blood vessel growth in the fertilized chicken eggs at days 20 post implantation [81]. Furthermore, The Cu/a-C:H films showed no invading polymorphonuclear leukocytes (PML) inside the implants.

4. Conclusions

Multifunctional Cu/a-C:H sputter-coated thin films has been deposited on the Ti-6Al-4V alloy in a gaseous mixture of Ar and CH_4. The effect of the content of Cu and the ratio of sp^2/sp^3 ratio on the tribological, microstructure, mechanical, anti-corrosion and biocompatibility behaviors have been analyzed. Increase of Ar/CH_4 ratio in the sputtering chamber resulted in thin films with higher sp^2/sp^3 ratios with enlarged graphitic domains. As the content of Cu increased, lower internal stress remained in the coatings. Smaller grains with higher densities were the result of lower Cu content and sp^2/sp^3 ratio. It seems that there is an optimum sp^2 fraction and graphitic domain sizes in Cu/a-C:H thin films which results in good mechanical properties and high corrosion resistance. Furthermore, the coated samples inhibited the growth of bacteria as compared to the uncoated sample ($p < 0.05$). In addition, such coating composition can stimulate angiogenesis, osteogenesis and control host response, thereby increasing the success rate of implants. Cu-enriched Cu/a-C:H coatings showed improved antibacterial properties, as well as higher angiogenesis and osteogenesis activities. Moreover, Cu/a-C:H thin films assisted in development of blood vessels on the surface of titanium alloy, particularly when the density of grown blood vessels was higher. The results of this survey accentuate the importance of controlling the atmosphere and the microstructure of Cu/a-C:H thin films to have an implant with optimized properties. It is speculated that such coating can be a promising candidate for enhancing the osseointegration features.

Declarations

Author contribution statement

Peiman Brouki Milan & Henri Vahabi: Performed the experiments; Wrote the paper.

Sara Khamseh: Performed the experiments.

Payam Zarrintaj: Contributed reagents, materials, analysis tools or data; Wrote the paper.

Bahram Ramezanzadeh & Michael Badawi: Analyzed and interpreted the data.

Sophie Morisset: Analyzed and interpreted the data; Contributed reagents, materials, analysis tools or data.

Mohammad Reza Saeb & Masoud Mozafari: Conceived and designed the experiments; Analyzed and interpreted the data; Contributed reagents, materials, analysis tools or data.

Funding statement

This research did not receive any specific grant from funding agencies in the public, commercial, or not-for-profit sectors.

Competing interest statement

The authors declare no conflict of interest.

Additional information

No additional information is available for this paper.

References

[1] L. Yate, L.E. Coy, D. Gregurec, W. Aperador, S.E. Moya, G. Wang, Nb–C nanocomposite films with enhanced biocompatibility and mechanical properties for hard-tissue implant applications, ACS Appl. Mater. Interfaces 7 (11) (2015) 6351–6358.

[2] S. Mohebbi, et al., Chitosan in biomedical engineering: a critical review, Curr. Stem Cell Res. Ther. 14 (2) (2019) 93–116.

[3] A. Samadi, R. Hasanzadeh, T. Azdast, H. Abdollahi, P. Zarrintaj, M.R. Saeb, Piezoelectric Performance of Microcellular Polypropylene Foams Fabricated Using Foam Injection Molding as a Potential Scaffold for Bone Tissue Engineering, Part B, J. Macromol. Sci. Part B (2020) 1–14. In press.

[4] M. Mozafari, S. Kargozar, S. Ramakrishna, Chemistry of biomaterials: future prospects, Curr. Opin. Biomed. Eng. 10 (2019) 181–190.

[5] A. Nemati, M. Saghafi, S. Khamseh, E. Alibakhshi, P. Zarrintaj, M.R. Saeb, Magnetron-sputtered Ti x N y thin films applied on titanium-based alloys for biomedical applications: composition-microstructure-property relationships, Surface Coatings Technol. 349 (2018) 251–259.

[6] M. Sadeghi-Kiakhani, S. Khamseh, A. Rafie, S.M.F. Tekieh, P. Zarrintaj, M.R. Saeb, Thermally stable antibacterial wool fabrics surface-decorated by TiON and TiON/Cu thin films, Surface Innovat. 6 (4–5) (2018) 258–265.

[7] R. Khalili, P. Zarrintaj, S.H. Jafari, H. Vahabi, M.R. Saeb, Electroactive poly (p-phenylene sulfide)/r-graphene oxide/chitosan as a novel potential candidate for tissue engineering, Int. J. Biol. Macromol. 154 (2020) 18–24. https://www.sciencedirect.com/science/article/pii/S0141813019391469.

[8] M. Rahmati, M. Mozafari, Nano-immunoengineering: opportunities and challenges, Curr. Opin. Biomed. Eng. 10 (2019) 51–59.

[9] J.J. Green, J.H. Elisseeff, Mimicking biological functionality with polymers for biomedical applications, Nature 540 (7633) (2016) 386.

[10] P. Zarrintaj, M.R. Saeb, S. Ramakrishna, M. Mozafari, Biomaterials selection for neuroprosthetics, Curr. Opin. Biomed. Eng. (2018).

[11] R.K. Schenk, D. Buser, Osseointegration: a reality, Periodontology 2000 17 (1) (1998) 22–35.

[12] M. Rahmati, A. Mobasheri, M. Mozafari, Inflammatory mediators in osteoarthritis: a critical review of the state-of-the-art, current prospects, and future challenges, Bone 85 (2016) 81–90.

[13] G. Mahmodi, et al., From microporous to mesoporous mineral frameworks: an alliance between zeolite and chitosan 489 (2020) 107930.

[14] B. Bakhshandeh, et al., Tissue engineering; strategies, tissues, and biomaterials, Biotechnol. Genet. Eng. Rev. 33 (2) (2017) 144–172.

[15] R. Langer, M.W. Tibbitt, Living biomaterials, Accounts Chem. Res. 50 (3) (2017) 508–513.

[16] D. Jianxun, Electrospun polymer biomaterials, Prog. Polym. Sci. 90 (2019) 1–34.

[17] M. Shoichet, et al., Polymer scaffolds for biomaterials applications, Macromolecules 43 (2) (2010) 581–591.

[18] S. Manouchehri, et al., Electroactive bio-epoxy incorporated chitosan-oligoaniline as an advanced hydrogel coating for neural interfaces, Prog. Org. Coating 131 (2019) 389–396.

[19] S. Khamseh, et al., High-performance hybrid coatings based on diamond-like carbon and copper for carbon steel protection, Diam. Relat. Mater. 80 (2017) 84–92.

[20] J. Russell, J. Hasan, E.P. Ivanova, Antibacterial surfaces: the quest for a new generation of biomaterials, Trends Biotechnol. 31 (5) (2013) 295–304.

[21] P. Zarrintaj, et al., Oligoaniline-based conductive biomaterials for tissue engineering, Acta Biomater. 72 (2018) 16–34.

[22] M. Servatan, et al., Zeolites in Drug Delivery: Progress, Challenges and Opportunities, 2020.

[23] B. Bagheri, et al., Self-gelling electroactive hydrogels based on chitosan–aniline oligomers/agarose for neural tissue engineering with on-demand drug release 184 (2019) 110549.

[24] P. Zarrintaj, B. Bakhshandeh, I. Rezaeian, B. Heshmatian, M.R. Ganjali, A novel electroactive agarose-aniline pentamer platform as a potential candidate for neural tissue engineering, Sci. Rep. 7 (1) (2017) 17187.

[25] P. Zarrintaj, A. Urbanska, S.S. Gholizadeh, V. Goodarzi, M.R. Saeb, M. Mozafari, A facile route to the synthesis of anilinic electroactive colloidal hydrogels for neural tissue engineering applications, J. Colloid Interface Sci. (2018).

[26] R. Langer, et al., Designing materials for biology and medicine, Nature 428 (6982) (2004) 487–492.

[27] Z. Bagher, et al., Conductive hydrogel based on chitosan-aniline pentamer/gelatin/agarose significantly promoted motor neuron-like cells differentiation of human olfactory ecto-mesenchymal stem cells, Mater. Sci. Eng. C (2019).

[28] Z. Atoufi, P. Zarrintaj, G.H. Motlagh, A. Amiri, Z. Bagher, S.K. Kamrava, A novel bio electro active alginate-aniline tetramer/agarose scaffold for tissue engineering: synthesis, characterization, drug release and cell culture study, J. Biomater. Sci. Polym. Ed. 28 (15) (2017) 1617–1638.

[29] M.A. Nilforoushzadeh, et al., Engineering the niche for hair regeneration–a critical review, Nanomed. Nanotechnol. Biol. Med. (2018).

[30] R. Alizadeh, et al., Conductive hydrogels based on agarose/alginate/chitosan for neural disorder therapy 224 (2019) 115161.

[31] M.R. Derakhshandeh, et al., Diamond-like carbon thin films prepared by pulsed-DC PE-CVD for biomedical applications, Surface Innovat. 6 (3) (2018) 167–175.

[32] S.M.R. Derakhshandeh, et al., Diamond-like carbon-deposited films: a new class of bio-corrosion protective coatings, Surface Innovat. (2018) 1–42.

[33] S. Khamseh, et al., Magnetron-sputtered copper/diamond-like carbon composite thin films with super anti-corrosion properties, Surf. Coating. Technol. 333 (2018) 148–157.

[34] S. Khamseh, et al., Magnetron-sputtered Copper/Diamond-like Composite Thin Films with Super Anti-corrosion Properties, 2017.

[35] A.B. Khiabani, A. Ghanbari, B. Yarmand, A. Zamanian, M. Mozafari, Improving corrosion behavior and in vitro bioactivity of plasma electrolytic oxidized AZ91 magnesium alloy using calcium fluoride containing electrolyte, Mater. Lett. 212 (2018) 98–102.

[36] G. Stachowiak, A.W. Batchelor, Engineering Tribology, Butterworth-Heinemann, 2013.

[37] M. Mozafari, E. Salahinejad, S. Sharifi-Asl, D. Macdonald, D. Vashaee, L. Tayebi, Innovative surface modification of orthopaedic implants with positive effects on wettability and in vitro anti-corrosion performance, Surf. Eng. 30 (9) (2014) 688–692.

[38] M.-Y. Tsai, et al., Surface properties of copper-incorporated diamond-like carbon films deposited by hybrid magnetron sputtering, Ceram. Int. 39 (7) (2013) 8335–8340.

[39] R. Bayón, A. Igartua, J. González, U.R. de Gopegui, Influence of the carbon content on the corrosion and tribocorrosion performance of Ti-DLC coatings for biomedical alloys, Tribol. Int. 88 (2015) 115–125.

[40] M. Azzi, P. Amirault, M. Paquette, J. Klemberg-Sapieha, L. Martinu, Corrosion performance and mechanical stability of 316L/DLC coating system: role of interlayers, Surf. Coating. Technol. 204 (24) (2010) 3986–3994.

[41] F. Heidenau, et al., A novel antibacterial titania coating: metal ion toxicity and in vitro surface colonization, J. Mater. Sci. Mater. Med. 16 (10) (2005) 883–888.

[42] T. Shirai, H. Tsuchiya, T. Shimizu, K. Ohtani, Y. Zen, K. Tomita, Prevention of pin tract infection with titanium-copper alloys, J. Biomed. Mater. Res. B Appl. Biomater. 91 (1) (2009) 373–380.

[43] K. Page, M. Wilson, I.P. Parkin, Antimicrobial surfaces and their potential in reducing the role of the inanimate environment in the incidence of hospital-acquired infections, J. Mater. Chem. 19 (23) (2009) 3819–3831.

[44] K. Page, R.G. Palgrave, I.P. Parkin, M. Wilson, S.L. Savin, A.V. Chadwick, Titania and silver–titania composite films on glass—potent antimicrobial coatings, J. Mater. Chem. 17 (1) (2007) 95–104.

[45] C. Castro, R. Sanjines, C. Pulgarin, P. Osorio, S. Giraldo, J. Kiwi, Structure–reactivity relations for DC-magnetron sputtered Cu-layers during E. coli inactivation in the dark and under light, J. Photochem. Photobiol. Chem. 216 (2) (2010) 295–302.

[46] Y. Liu, P. Guo, X. He, L. Li, A. Wang, H. Li, Developing transparent copper-doped diamond-like carbon films for marine antifouling applications, Diam. Relat. Mater. 69 (2016) 144–151.

[47] N. Dwivedi, et al., Investigation of properties of Cu containing DLC films produced by PECVD process, J. Phys. Chem. Solid. 73 (2) (2012) 308–316.

[48] X. Yu, Z. Ning, M. Hua, C. Wang, F. Cui, Mechanical and biomedical properties of copper-containing diamond-like carbon films on magnesium alloys, J. Mater. Chem. B 1 (37) (2013) 4773–4780.

[49] J. Zhou, L. Zhao, Hypoxia-mimicking Co doped TiO2 microporous coating on titanium with enhanced angiogenic and osteogenic activities, Acta Biomater. 43 (2016) 358–368.

[50] P.C. Ha, D. McKenzie, M. Bilek, S. Kwok, P. Chu, B. Tay, Raman spectroscopy study of DLC films prepared by RF plasma and filtered cathodic arc, Surf. Coating. Technol. 201 (15) (2007) 6734–6736.

[51] N. Kharlamova, et al., Antibodies to Porphyromonas gingivalis indicate interaction between oral infection, smoking, and risk genes in rheumatoid arthritis etiology, Arthritis Rheumatol. 68 (3) (2016) 604–613.

[52] H.W. Choi, J.-H. Choi, K.-R. Lee, J.-P. Ahn, K.H. Oh, Structure and mechanical properties of Ag-incorporated DLC films prepared by a hybrid ion beam deposition system, Thin Solid Films 516 (2) (2007) 248–251.

[53] S. Wei, W. Kang, J. Davidson, J. Huang, Aligned carbon nanotubes fabricated by thermal CVD at atmospheric pressure using Co as catalyst with NH 3 as reactive gas, Diam. Relat. Mater. 15 (11) (2006) 1828–1833.

[54] L. Ji, H. Li, F. Zhao, J. Chen, H. Zhou, Microstructure and mechanical properties of Mo/DLC nanocomposite films, Diam. Relat. Mater. 17 (11) (2008) 1949–1954.

[55] Y.-H. Chan, C.-F. Huang, K.-L. Ou, P.-W. Peng, Mechanical properties and antibacterial activity of copper doped diamond-like carbon films, Surf. Coating. Technol. 206 (6) (2011) 1037–1040.

[56] Q. Wei, A. Sharma, J. Sankar, J. Narayan, Mechanical properties of diamond-like carbon composite thin films prepared by pulsed laser deposition, Compos. B Eng. 30 (7) (1999) 675–684.

[57] C.-C. Chen, F.C.-N. Hong, Structure and properties of diamond-like carbon nanocomposite films containing copper nanoparticles, Appl. Surf. Sci. 242 (3) (2005) 261–269.

[58] J. Musil, H. Polakova, Hard nanocomposite Zr–Y–N coatings, correlation between hardness and structure, Surf. Coating. Technol. 127 (1) (2000) 99–106.

[59] F. Regent, J. Musil, Magnetron sputtered Cr Ni N and Ti Mo N films: comparison of mechanical properties, Surf. Coating. Technol. 142 (2001) 146–151.

[60] S. Veprek, et al., Limits to the strength of super-and ultrahard nanocomposite coatings, J. Vac. Sci. Technol.: Vacuum Surfaces Films 21 (3) (2003) 532–544.
[61] Y. Pauleau, F. Thiery, V. Uglov, V. Anishchik, A. Kuleshov, M. Samtsov, Tribological properties of copper/carbon films formed by microwave plasma-assisted deposition techniques, Surf. Coating. Technol. 180 (2004) 102–107.
[62] H. Xie, Y.J. Kang, Role of copper in angiogenesis and its medicinal implications, Curr. Med. Chem. 16 (10) (2009) 1304–1314.
[63] L.D. D'Andrea, A. Romanelli, R. Di Stasi, C. Pedone, Bioinorganic aspects of angiogenesis, Dalton Trans. 39 (33) (2010) 7625–7636.
[64] N. Kong, K. Lin, H. Li, J. Chang, Synergy effects of copper and silicon ions on stimulation of vascularization by copper-doped calcium silicate, J. Mater. Chem. B 2 (8) (2014) 1100–1110.
[65] E. Schipani, C. Maes, G. Carmeliet, G.L. Semenza, Regulation of osteogenesis-angiogenesis coupling by HIFs and VEGF, J. Bone Miner. Res. 24 (8) (2009) 1347–1353.
[66] F. Marciano, L. Bonetti, N. Da-Silva, E. Corat, V. Trava-Airoldi, Wettability and antibacterial activity of modified diamond-like carbon films, Appl. Surf. Sci. 255 (20) (2009) 8377–8382.
[67] J. Wang, et al., Bacterial repellence from polyethylene terephthalate surface modified by acetylene plasma immersion ion implantation–deposition, Surf. Coating. Technol. 186 (1-2) (2004) 299–304.
[68] H.-f. Chen, J.-j. Wu, M.-y. Wu, H. Jia, Preparation and antibacterial activities of copper nanoparticles encapsulated by carbon, N. Carbon Mater. 34 (4) (2019) 382–389.
[69] A. Javid, M. Kumar, S. Yoon, J.H. Lee, J.G. Han, Synergistic enhancement of antibacterial activity of Cu: C nanocomposites through plasma induced microstructural engineering, Appl. Surf. Sci. 500 (2020) 143996.
[70] J. Li, Y. Qiao, H. Zhu, F. Meng, X. Liu, Existence, release, and antibacterial actions of silver nanoparticles on Ag–PIII TiO2 films with different nanotopographies, Int. J. Nanomed. 9 (2014) 3389.
[71] A.K. Chatterjee, R. Chakraborty, T. Basu, Mechanism of antibacterial activity of copper nanoparticles, Nanotechnology 25 (13) (2014) 135101.
[72] I. Burghardt, et al., A dual function of copper in designing regenerative implants, Biomaterials 44 (2015) 36–44.
[73] C. Wu, et al., Copper-containing mesoporous bioactive glass scaffolds with multifunctional properties of angiogenesis capacity, osteostimulation and antibacterial activity, Biomaterials 34 (2) (2013) 422–433.
[74] H. Zhou, L. Xu, A. Ogino, M. Nagatsu, Investigation into the antibacterial property of carbon films, Diam. Relat. Mater. 17 (7-10) (2008) 1416–1419.
[75] P. Zarrintaj, Z. Ahmadi, H. Vahabi, F. Ducos, M.R. Saeb, M. Mozafari, Polyaniline in retrospect and prospect, Mater. Today Proc. 5 (7) (2018) 15852–15860.
[76] A. Pier-Francesco, R.J. Adams, M.G. Waters, D.W. Williams, Titanium surface modification and its effect on the adherence of Porphyromonas gingivalis: an in vitro study, Clin. Oral Implants Res. 17 (6) (2006) 633–637.
[77] B. Li, B.E. Logan, Bacterial adhesion to glass and metal-oxide surfaces, Colloids Surfaces B Biointerfaces 36 (2) (2004) 81–90.
[78] E.D. Harris, A requirement for copper in angiogenesis, Nutr. Rev. 62 (2) (2004) 60–64.
[79] M. Takamura, et al., Loss of liver-intestine cadherin in human intrahepatic cholangiocarcinoma promotes angiogenesis by up-regulating metal-responsive transcription factor-1 and placental growth factor, Int. J. Oncol. 36 (1) (2010) 245–254.
[80] G. Narayanan, S. Bharathidevi, H. Vuyyuru, B. Muthuvel, S.K. Natrajan, CTR1 silencing inhibits angiogenesis by limiting copper entry into endothelial cells, PloS One 8 (9) (2013), e71982.
[81] N. Mroczek-Sosnowska, et al., Nanoparticles of copper stimulate angiogenesis at systemic and molecular level, Int. J. Mol. Sci. 16 (3) (2015) 4838–4849.